ARTICLE

Check for updates

Improved prediction of the vertical distribution of ground ice in Arctic-Antarctic permafrost sediments

Denis Lacelle [1✉], David A. Fisher[2], Marjolaine Verret [3] & Wayne Pollard [4]

Global warming and permafrost degradation are impacting landscapes, ecosystems and the climate-carbon system. Current ground ice and geohazard maps rely on the frost susceptibility of surficial sediments, and substantial areas underestimate ice abundance. Here we use a soil environmental model to show the importance of considering unfrozen water content (dependent on sediment type, soil water chemistry, and temperature) when assessing the frost susceptibility of sediments. Our ensemble modeling of the vertical structure and evolution of ground ice for fine to coarse-grained sediments matches reasonably well with field measurements at sites from the low Arctic to the cold and hyper-arid Dry Valleys of Antarctica. Our modeling indicates a need to re-evaluate how frost-susceptible sediments are identified when mapping ice-rich permafrost landscapes and provides a framework for the development of quantitative estimates of the vertical distribution of ground ice in permafrost sediments at regional scale.

[1] Department of Geography Environment and Geomatics, University of Ottawa, Ottawa, ON K1N 6N5, Canada. [2] Department of Earth Sciences, University of Ottawa, Ottawa, ON, Canada. [3] Antarctic Research Centre, Victoria University of Wellington, Wellington 6011, New Zealand. [4] Department of Geography, McGill University, Montreal, QC H3A 0G4, Canada. ✉email: dlacelle@uottawa.ca

Permafrost has attracted tremendous attention from the scientific community and society over the past decades[1]. Global warming and permafrost degradation are impacting all aspects of polar landscapes, including: infrastructure, vegetation assemblage and ecosystems[2], lakes and rivers[3], and soil biogeochemical cycles[4]. Additionally, with the microbial decomposition of large stocks of organic carbon, permafrost degradation is contributing to a positive feedback in the global climate-carbon system[5,6]. However, the nature and magnitude of these changes are dependent on the vertical distribution of ice in permafrost sediments. Ground ice (particularly excess ice) controls the rate of permafrost degradation due to its high latent heat and the complex nature of potential feedbacks of thawing icy permafrost. For example, the positive feedbacks that develop following differential thaw of icy permafrost and ponding of the melted ice[7,8]. There is therefore a need to improve our knowledge on the factors influencing the vertical distribution of ground ice in the complex permafrost system in different landscapes to better assess the ongoing environmental changes and geohazard risks[9,10].

There are four main types of ground ice in permafrost: pore ice, vein ice, buried surface ice, and intrasedimental ice (which includes segregated ice)[11,12]. Pore ice refers to the in situ freezing of soil moisture and tends to cement permafrost sediments; vein ice (ice wedges) is associated with frost cracking and is recognizable from polygonal patterned terrain, whereas the burial of surface ice is site-specific and relates mainly to glacial limits. In the absence of direct cryostratigraphic observations, the spatial and vertical distribution of intrasedimental ice is challenging to constrain, even when using remote sensing techniques[13]. As a result, studies often rely on sediment types to infer the abundance of intrasedimental ice: fine-grained sediments are classified as "frost-susceptible" and are inferred to be ice-rich and prone to geohazards[14]. For example, the ground ice map of Canada classified large areas as ice-rich permafrost with segregated ice based on surficial sediments and their frost susceptibility[15,16] (Fig. 1). A similar map classified ice-free regions of South Victoria Land of Antarctica, including the McMurdo Dry Valleys (MDV), almost entirely as dry permafrost due to the coarse nature of the sediments, hyper-arid climate, and age of the surficial deposits[17] (Fig. 1). However, for example, clast-rich tills in the Richardson Mountains/Peel Plateau region in the Northwest Territories[18,19], muck deposits in the Klondike region in Yukon[20,21], fluvial gravels in the Mackenzie Delta[22,23], silty colluvium near Salluit in Nunavik[24] and sandy-stony sediments in the MDV[25–27] often contain ground ice abundance similar to frost-susceptible soils, but were identified as regions with low-medium ice content. This suggests that there are factors other than particle size, sediment age, and climate that can lead to near-surface ice enrichment.

In this study, we first review the temperature, salinity, and vertical distribution of intrasedimental ice in Arctic and Antarctic permafrost sediments, including organic-rich soils. Then, we determine the unfrozen water content profiles (S_L) for different sediment types and water chemistries using the SOIL8MIN model[28]. Laboratory measurements and modeling have shown that the pore water ($S_L > \sim0.13$) can migrate under thermal and pressure gradients induced by temperature cycles in the permafrost sediments (here referred as rheological forces or REGO); whereas the film water ($S_L < \sim0.13$) can move under Van der Walls (VdW) forces (i.e., a pressure gradient within the film of water around soil particles that is dependent on temperature, radius of soil particles and the Hamaker constant)[29–32]. The REGO forces are also the ones that produce surface tension cracks and patterned ground, and the VDW forces produce segregation ice and frost heaving. Once S_L is determined, we quantify the seasonality in the direction and speed of water migration under REGO and VdW forces in permafrost sediments with the WATEREGO model and, based on the ensemble results, determine the redistribution over time of ground ice in a deep permafrost column[28]. The model uses 17 ensemble parameters that reflect the modern regional permafrost and environmental conditions, and the final computation represents the average of 18 to 54 realizations. Together, this allows us to determine the effects of REGO or VdW forces on moving the unfrozen water in permafrost sediments with varying temperatures and salinities, and the rate at which ice can accumulate in the near-surface permafrost. Overall, this study provides the framework to develop a quantitative assessment of the vertical distribution of intrasedimental ice in permafrost sediments, a product that would improve environmental and geohazard risk assessments.

Results and Discussion

Arctic and Antarctic permafrost sediments: temperature, salinity, and ground ice. Permafrost is defined as a thermal condition of the ground where the sediments or bedrock remains below 0 °C for two or more consecutive years[33]. However, when permafrost contains ice, it can be described as the ground that remains *frozen* for two or more consecutive years[34]. The thickness of the active layer may equal, but generally exceeds the maximum depth of the 0 °C isotherm due to soil water salinity and the associated freezing point depression[34,35]. In the Arctic, the active layer is often moist to water-saturated and the boundary between the active layer and underlying permafrost is termed the permafrost table[36]. However, in the cold hyper-arid regions of Antarctica, the sediments above the ice-bearing permafrost are often dry[37–39]. Similar to the Arctic, the near-surface dry sediments in Antarctica may warm above 0 °C due to solar heating and develop an active layer[40,41]. If the depth to the icy permafrost exceeds the depth of 0 °C isotherm, that zone is termed dry permafrost with the boundary between the dry and icy permafrost called the ice table[42]. Therefore, in cold hyper-arid regions, the permafrost table represents the depth of the 0 °C isotherm, and the ice table represents a sublimation unconformity[43]. The depth of the permafrost table (0 °C isotherm or thaw unconformity) can be estimated from heat conduction equations (such as the Stefan equation)[44], whereas the depth of the ice table (sublimation unconformity) can be estimated using the water vapor density gradient between the ground surface and the ice-bearing ground[45–48].

In permafrost regions of the Canadian Arctic, the mean annual air temperature (MAAT) and precipitation display a broad latitudinal gradient with relatively warmer-wetter conditions in low Arctic regions and colder-dryer conditions in the high Arctic; thaw degree-days range from ~2000 in the low Arctic to ~250 in the high Arctic[49] (Fig. 1). The mean annual temperatures at the permafrost table range from near 0 °C in discontinuous permafrost to ~–15 °C in the continuous permafrost of the high Arctic[50]. Knowledge of the chemical composition of ground ice in permafrost sediments is scarce. Studies from the Richardson Mountains to the Inuvik region shows that the melted ground ice has a $Ca(Mg)SO_4$ geochemical facies with solute load averaging 6.8 mg kg^{-1} soils[19,51]; conversely, the ground ice within the post-glacial marine limit often contains high NaCl, such as near Salluit in the Nunavik region, and in the coastal region of the Eureka Sound Lowlands[24,52,53] (Fig. 1). Permafrost in the Canadian Arctic is relatively young and largely reflects the late Quaternary post-glacial history[54,55]. The vertical distribution of ground ice in permafrost sediments were initially assessed from shot holes drilled for seismic studies as part of oil and gas exploration in the 1970s[56,57]. The qualitative distribution of ground ice (presence and thickness) in a variety of surficial deposits from the western Arctic (Richardson Mountains–Peel Plateau region and Richard
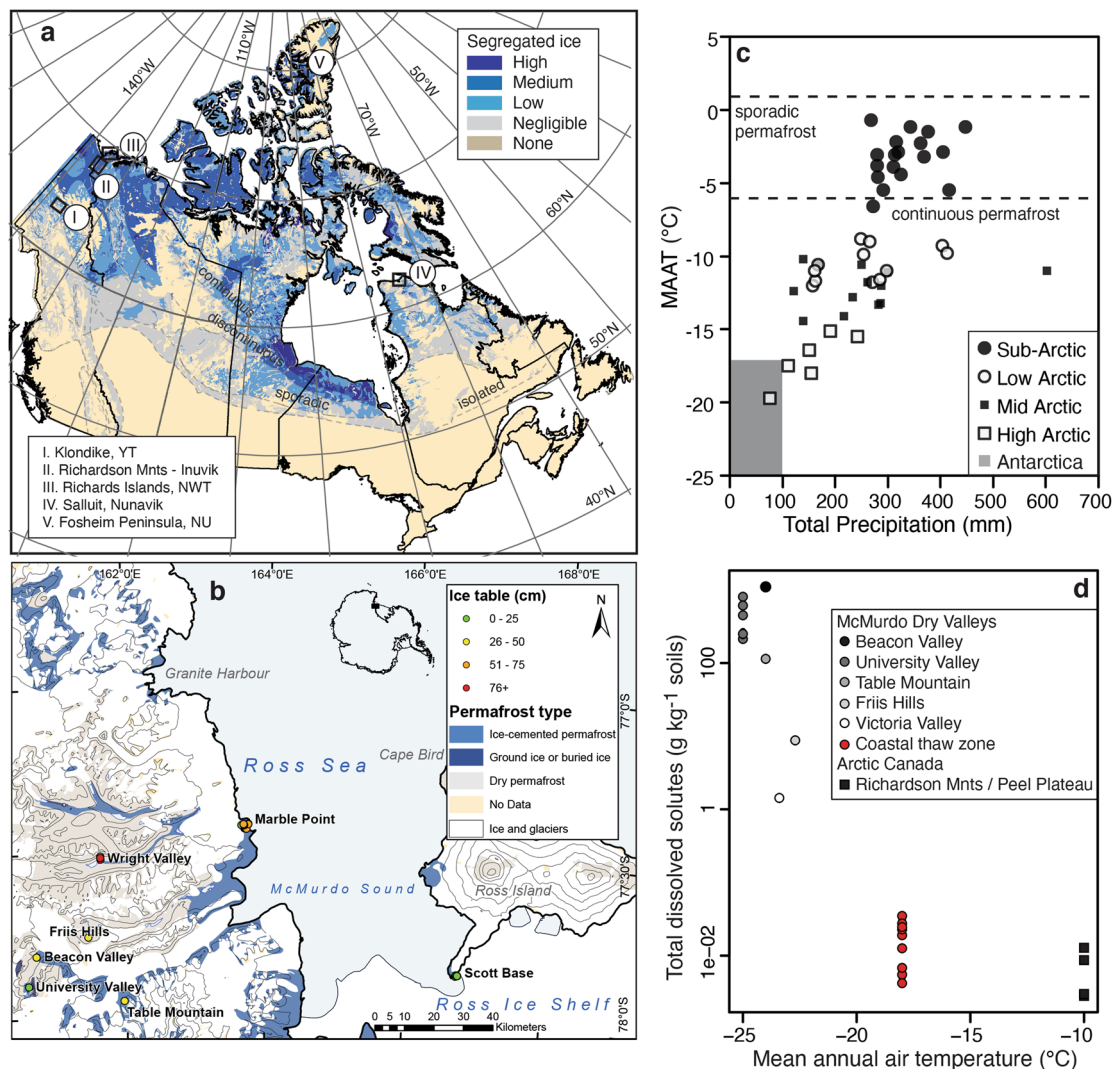
Fig. 1 Ground ice maps of and climate conditions in Arctic Canada and South Victoria Land region of Antarctica. a Map of segregation ice abundance of Arctic Canada (data from ref. [16]) and location of sampling sites mentioned in the text. **b** Map of ground ice and permafrost type in South Victoria Land region of Antarctica (data from ref. [17]) and location of sampling sites mentioned in the text. **c** Climate conditions in Arctic Canada and McMurdo Dry Valleys of Antarctica (data from refs. [85,86]). **d** Relation between total dissolved solutes in ground ice within permafrost of different regions of Arctic Canada and McMurdo Dry Valleys of Antarctica.

Island, NWT) and the high Arctic (Fosheim Peninsula, NU) showed that the uppermost 1–2 m was typically ice-rich (Fig. 2). This was later confirmed by measurements of ground ice content from permafrost cores (Fig. 2). The gravimetric water content (GWC) shows significant intra-site variations, but the uppermost section of permafrost at all sites is generally ice-rich (with excess ice) and some sites also display an ice-rich zone at ~4–5 m depth. Perennially frozen peat, and frozen organic material in general, contain a much higher ground ice content than permafrost soils due to its higher porosity (sometimes exceeding 96%$_{vol}$) and the higher water-absorbing capacity of organics (Fig. 2; Supplementary Data 1). Frozen peat, similar to permafrost soils, also displays zones of higher ice content, typically near the top of the frozen peat and ~2 m depth.

The MDV are the largest ice-free area of Antarctica and is classified as a cold and hyper-arid desert[58] (Fig. 1). In the coastal thaw zone, the MAAT ranges from –15 to –20 °C (~44 thaw degree-days) and precipitation approaches 100 mm snow water equivalent (swe); whereas in the stable upland zone at higher elevation, the MAAT and precipitation decreases to –20 to –25 °C (0 thaw degree-days) and <10 mm swe, respectively[59,60]. The

predominant surficial material is glacial till, usually with sandy to silty matrices, that range in age from Holocene to mid-Miocene[61]. The absence of vegetation and organic matter, reduced snow cover, and dry near-surface sediments (causing little to no seasonal change in thermal conductivity) ensure that the mean annual temperatures at the top of permafrost approximate the MAATs[62,63]. Salinity is an important property of sediments in the MDV. Since potential ablation exceeds precipitation, salts that are deposited by precipitation of snow or that are released during weathering of soils slowly accumulate in the sediments[64]. Salt types include sodium, potassium, and magnesium chlorides, nitrates, sulfates, and carbonates[65]. It was observed that salt concentrations increase with sediment age, but the colder-drier regions also contain higher salt abundances, reaching up to 1100 g kg^{-1} sediments[26], because of the paucity of liquid water (Fig. 1). This salt load is up to four orders of magnitude higher than in most Arctic permafrost sediments. In the MDV, hundreds of sites from the coastal thaw zone to the stable upland zone were investigated for ground ice content and sediment properties as part of the New Zealand Landcare Research (formerly the Soil Bureau) sampling campaigns in South Victoria Land from the
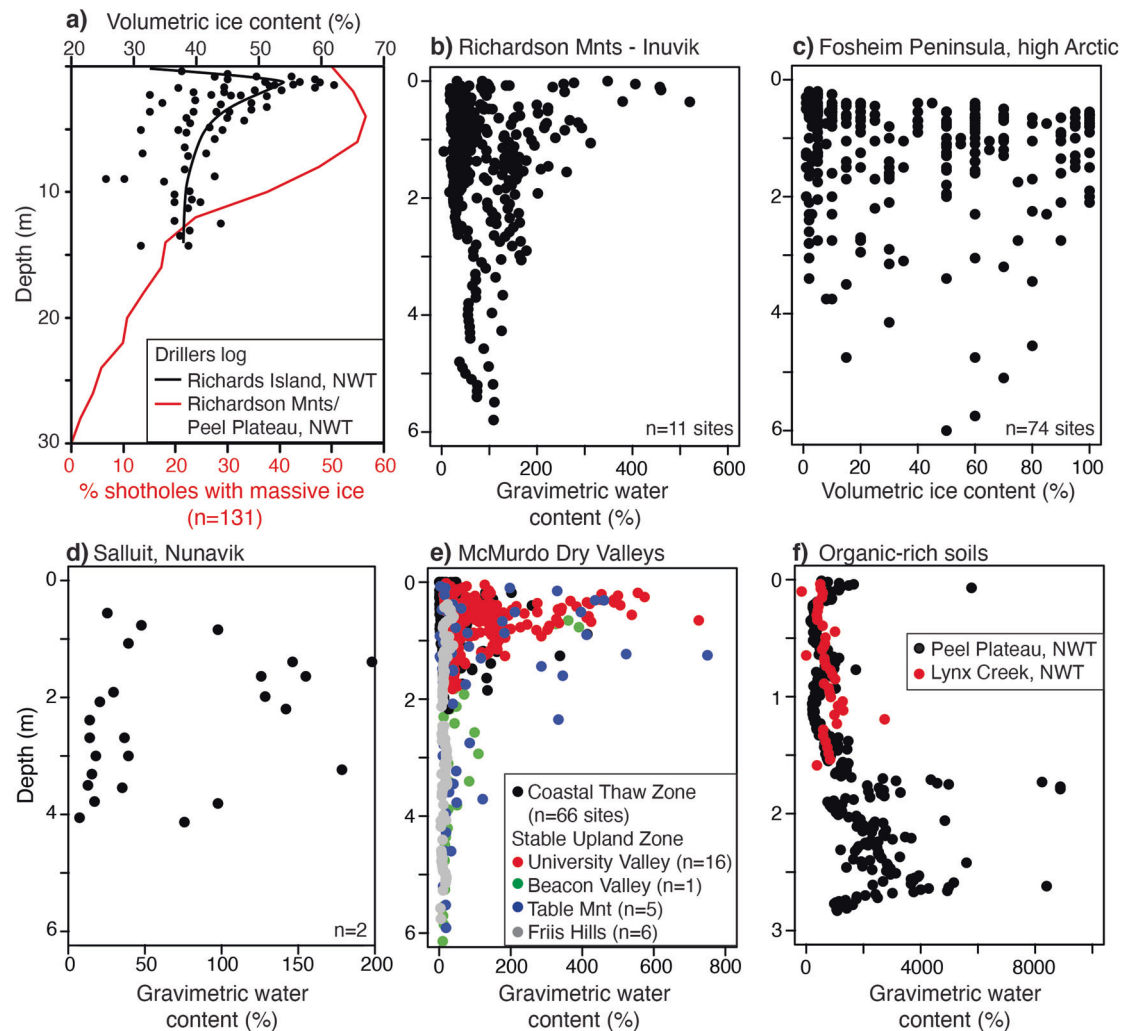
Fig. 2 Vertical distribution of ground ice at hundreds of sites in Arctic Canada and McMurdo Dry Valleys, Antarctica. a Ground ice abundance derived from seismic shotholes in western Arctic Canada (low Arctic). **b** Gravimetric water content from 11 sites in the Richardson Mountains and Inuvik region (low Arctic). **c** Gravimetric water content from 74 sites in the Fosheim Peninsula region (high Arctic). **d** Gravimetric water content from 2 sites in Northern Quebec (low Arctic). **e** Gravimetric water content from 94 sites in the McMurdo Dry Valleys of Antarctica. **f** Gravimetric water content from 2 sites with organic-rich soils. See Fig. 1 for locations of sites and methods for source of data.

1960s to 1990s[38,66–68]. The GWC of permafrost in the coastal thaw zone averaged 30.2 ± 40.0% (Fig. 2) and this led to permafrost being classified mostly as dry permafrost or ice-cemented permafrost throughout the MDV[17]. However, the addition of new sites from various research groups over the past two decades indicate that many sites at higher elevations display a zone of ice-enrichment below the ice table that extends to 1–2 m depth; below that depth, the GWC remains <30% with the exception of discrete ice lenses[25–27,69,70] (Fig. 2). In the two deep cores from icy permafrost soils (Beacon Valley and Friis Hills), ice-enrichment is also observed at ~5 m[26,27]. Approximately 70% of the surveyed sites in the stable upland zone ($n = 28$) have excess ice in the uppermost 2 m below the ice table.

Unfrozen water content and its seasonal migration in permafrost sediments. The in situ development of ice-rich zones in permafrost sediments requires the presence of unfrozen water that migrates to a freezing front[71]. The unfrozen water content as a function of ground temperatures (S_L) was initially determined in salt-free permafrost sediments, and it was shown to be dependent on the specific surface area of sediments[72]. Later, Rempel et al. expanded the S_L function to include soil porosity, dry bulk density,

and soil water chemistry[73]. Here, we use the Rempel-type S_L curves (computed from SOIL8MIN model) that encompasses temperature, sediment type, and soil water salinity for four sediment types (Inuvik clay, Chena silt, Lebanon gravel, and Nagare peat; Table 1) and different soil water chemistry (1x and 0.5x sea water, 0.1 molality Ca(Mg)SO4 water and pure water; Table 2) (Fig. 3). For all sediments, the S_L at temperatures near 0 °C is determined by the freezing point suppression of the soil water solution (1× seawater = −2.03 °C; 0.5× sea water = −1.01 °C; 0.1 molality Ca(Mg)SO4 = −0.58 °C). Below that temperature, the capacity of clays to hold more water under higher surface tension dominates over the effect of soil water chemistry, even for high salinity waters. However, for low salinity silt to gravel sediments, the S_L curve approaches that determined by their specific surface area (i.e., Anderson and Tice S_L-type function). But at higher salinity, the S_L of these coarser sediments is determined by the soil water chemistry: for example, silt to gravel with brackish to saline waters can have S_L near that of clays at equal temperatures. In these coarse sediments with brackish to saline waters, the residual water is precipitating NaCl ·2H2O at its eutectic point of −23 °C, which then substantially reduces S_L at lower temperatures due to the incorporation of water in the hydrated salts. Peat appears to

Table 1 Values of parameters for the different sediments used in SOIL8MIN model to determine unfrozen water content (S_L), a semi-empirical model that includes the soil properties and the geochemical composition of soil water.

Soil	Dry porosity	β	T_p (°C)	ΔT_f	Hamaker constant	R_{soil} (μm)
Inuvik clay[1]	0.55	0.245	−0.01	0.01050	−6.32 E−18	1
Inuvik clay[1]	0.45	0.245	−0.06	0.05102	−6.32 E−18	1
Chena silt[1]	0.55	0.531	0.0	0.00657	−6.32 E−18	5
Chena silt[1]	0.45	0.531	−0.01	0.0140	−6.32 E−18	5
Lebanon gravel	0.45	0.408	−0.01	0.00137	−6.32 E−18	100
Nagare peat[2]	0.84	0.725	1E−5	0.02209	−6.32 E−17	10

Reference: 1. Adersland and Ladanyi (2004); 2. Nagare et al., (2012).
Hamaker constant for peat was estimated using the S_L profile published by Nagare et al. 2012 (ref.[84]).

Table 2 Values of soil water chemistry used in SOIL8MIN model to determine unfrozen water content (S_L), a semi-empirical model that includes the soil properties and the geochemical composition of soil water.

Ion	Seawater	Ca(Mg)SO₄
Na^+	0.4861	0.005
Mg^{2+}	0.05474	0.03
Ca^{2+}	0.01074	0.06
K^+	0.01058	0.003
Cl^-	0.56672	0.0003
SO_4^{2-}	0.02927	0.094
HCO_3^-	0.00238	0

values mol kg⁻¹ water, molality.

have a slightly different behavior in terms of S_L curves relative to the other sediments. The intrinsic properties of peat allow it to hold slightly more unfrozen water at temperatures <−2 °C and S_L in low salinity peat appears to be kept constant at 0.08 with further cooling. Therefore, S_L cannot be simplified by a single curve for each sediment type but instead consists of a range of possible curves that depend on soil water chemistry as well.

Temp/W and NEST are commonly used models to assess thermal and phase changes in permafrost sediments. However, these models do not include the migration of unfrozen water under REGO and VdW forces and its freezing in a permafrost column. Fisher et al. (2020) therefore developed WATEREGO to explore the direction and speed of migration of the residual unfrozen water in >30 m deep permafrost column. The unfrozen water in permafrost sediments can exist as pore ($S_L > \sim0.13$) or film water ($S_L < \sim0.13$)[74]. The rate of migration of pore water by REGO forces depends on the permeability of permafrost sediments (with reported values in the 10^{-11} to 10^{-15} m² range)[74]. When S_L is in the film water domain, permeability is reduced by up to 6–7 orders of magnitude and water can move under VdW forces, a pressure gradient within the film of water around sediments particles[73]. In the Inuvik clay, S_L is always >0.13, irrespective of soil salinity (Fig. 3). Conversely, for the Chena silt, Lebanon gravel, and Nagare peat, S_L is only > 0.13 when ground temperatures are >−1 °C for low salinity soils and >−7 °C for brackish to saline soil water chemistry (Fig. 3).

Figure 4 shows typical seasonal temperature, stress, and S_L variations, the maximum weekly REGO-induced water speeds, and mean annual REGO and VdW-induced water speeds within a 30 m permafrost column of Inuvik clay with Ca(Mg)SO₄ water chemistry for mean annual ground surface temperature (MAGST) = −5 °C, amplitude = 5 °C, and thermal diffusivity = 62 m² yr⁻¹. The S_L stays within the pore water domain ($S_L > 0.13$) throughout the full year in the entire 30 m permafrost column (Fig. 4c). The maximum weekly REGO-induced water speeds, moving water upwards, occur near the permafrost table 8 to 23 weeks after the spring equinox (4.2 and

1.8 m yr⁻¹ at 0 and 0.5 m, respectively; Fig. 4d) and the maximum speeds subsequently decrease with depth (reaches 0.0001 m yr⁻¹ at 10 m; Fig. 4e). At each modeled depth, the increase in water speeds lasts 5 to 8 weeks while occurring progressively later in the year at increasing depth. The direction of REGO-induced water movement is entirely upward in the upper few meters, whereas at depths >6 m, there is the beginning of a downward water movement, and at 10 m, the downward and upward water speeds are equal. The VdW-induced weekly water speeds (not shown on Fig. 4) are moving water downward from the ground surface: they reach a maximum speed of 7.58×10^{-5} m yr⁻¹ at 0.5 m between weeks 8 and 17 after the spring equinox and are reduced to 2.18×10^{-5} m yr⁻¹ at 2 m. As a result, the net water movement is upward in the upper 10 m whereas it is downward from 10 to 25 m. Considering that mean annual REGO-induced water speeds are 1.5 to 3 orders of magnitude higher than the VdW-induced ones in the top 8 m, for these simulated temperature-stress conditions, the REGO-forces produce most of the water motion in clay soils (Fig. 4f).

Figure 5 shows typical seasonal temperature, stress, and S_L variations and the maximum weekly VdW-induced water speeds and mean annual REGO and VdW-induced water speeds within a 30 m permafrost column of Chena silt with Ca(Mg)SO₄ water chemistry for the same conditions as for the Inuvik clay. The S_L is in the pore water domain (>0.13) only for 1–2 months in the uppermost 0.5 m (Fig. 5c). Therefore, unlike for the Inuvik clays where the bulk of the water migration is induced by REGO forces, VdW forces dominate water migration in the Chena silts. The maximum weekly VdW-induced forces that move water downwards occur 8 to 17 weeks after the spring equinox (7×10^{-4} and 0.75×10^{-4} m yr⁻¹ at depths of 0.5 and 2 m, respectively; Fig. 5d). Below 2 m, the water speeds are increasingly reduced and occur progressively later in the year (Fig. 5e). The VdW forces move the water downwards from the permafrost table to 8 m depth, and below that depth, water migration is upwards (Fig. 5f). The mean annual VdW-induced water speeds are higher than REGO-forces by a factor of 45–75 in the top 7 m and by a factor of 12–15 from 8 to 25 m depth. The water is moving upward at near-constant speed because of the greatly diminished seasonal temperature amplitude and the gradually warming trend with depth (input of the geothermal temperature gradient of 2 °C 100 m⁻¹). Increasing soil salinity (or the MAGST) would affect these findings for the Chena silt since it would increase the S_L at the same temperature and consequently increase the permeability and the water speeds. However, the water speeds would not reach those in the clays because S_L would be > 0.13 only at temperatures >−7 °C (Fig. 3). The seasonality in the direction and magnitude of water transport in silty (clayey-silts) sediments, with a net downward flux, has been confirmed from low Arctic regions by tritium measurements[75,76].

Predicting ground ice content profiles. The combined effects of the REGO and VdW forces on the movement of residual water
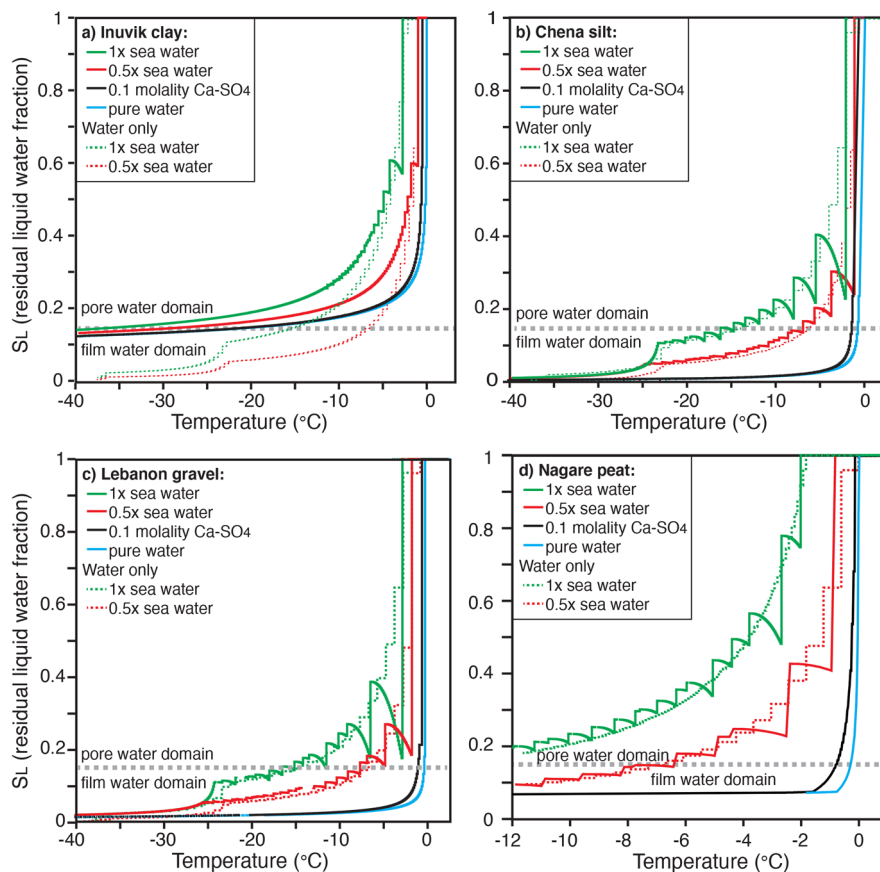
Fig. 3 Unfrozen water content profiles for various sediment types with varying soil water chemistry. The S_L profiles were computed using SOIL8MIN model[28]. **a** Inuvik clay, **b** Chena silt, **c** Lebanon gravel and **d** Nagare peat. The oscillations in the S_L curves are due to an instability in the use of the Rempel-type equation to determine the fraction of residual liquid water that would force the ground ice to completely melt, but SOIL8MIN limits the amount of ground ice that can melt based on a heat energy exchange (see eq. 12 in Fisher et al. 2020). The pore water ($S_L > {\sim}0.13$) and film water ($S_L < {\sim}0.13$) domains are illustrated as these determine the dominant process (REGO or VdW, respectively) by which the unfrozen water can migrate.

in permafrost sediments can modify the initial ground ice content profile and, over time, lead to zones of ice-enrichment and zones of ice-depletion. The evolution of ground ice profiles using WATEREGO is compared to the vertical distribution of ground ice at three sites with very different conditions: (1) Peel Plateau/Richardson Mountains, NWT, Canada (MAAT ~−10 °C, clayey-silt till, 0.1 molality Ca(Mg)SO$_4$ chemistry), (2) Friis Hills, upper MDV (MAAT –23 °C, sandy-silt diamict, 0.1× seawater chemistry) and (3) lower Beacon Valley, the upper MDV (MAAT –23 °C, sandy sediments, 0.2× seawater chemistry) (Fig. 6). For each site, the values of the input ensemble parameters were selected to approximate those measured in their respective region and are listed in Table 3. For the ensemble modeling, an initial ground ice profile is produced with downward freezing simulating permafrost aggradation in a water-saturated column of sediments. The initial profile (not shown) shows a high ground ice content in the uppermost 5 m (54%$_{vol}$), which then gradually decreases to 25%$_{vol}$ at 20 m depth. The seasonal ground temperature cycles then generate stress fields that initiate the migration of the residual unfrozen water at speeds determined by S_L and permeability and the REGO and the VdW forces. Due to uncertainties in the e-folding decay of the rate of ice buildup following the freezing of residual water (1/2e to 1/7e; ref. [28,31]), the negative depth derivatives of water speeds (dWS$_{REGO}$/dZ) are used to indicate where ice accumulates by freezing or is removed by melting. But as an example, the depth derivative of water speeds for the Navy Rd clayey silt and Inuvik clay mixture (50:50) were

converted to volumetric ice content for comparison with that on the Peel Plateau/Richardson Mountains.

The measured ground ice profiles at all three sites fit reasonably well with the ones predicted from the ensemble numerical simulations that assumes a homogenous permafrost column and do not account for stratigraphic layering or historical changes in ground temperatures. On the Peel Plateau/Richardson Mountains, both the modeling and measurements indicate ground ice accumulating just below the permafrost table and at 3–5 m, 11–13 m, 17–19 m, and 24–26 m depth intervals (Fig. 6a). At Friis Hills, ground ice accumulates just below the ice table and at ~15–20 m; however, the zone between 5–10 m has a low ice content, as predicted from the modeling (Fig. 6b note the change in scale for dWS$_{REGO}$/dZ). Finally, in lower Beacon Valley (Fig. 6c), both the modeling and measurements indicate an ice-rich zone just below the ice table with ice content increasing between 5 and 10 m (but remains below that near the ice table; note the change in scale for dWS$_{REGO}$/dZ). Below 10 m, ice-rich zones develop near 13–15 and 18–20 m. The ensemble modeling results suggest that the rate of ice accumulation in permafrost sediments is dependent on diffusivity, permeability, and S_L (and therefore on sediment type, water chemistry, and permafrost temperature). The rate is orders of magnitude faster near the permafrost/ice table than at depth due to the warmer ground temperatures (note S_L is an exponential function) and the combined effects of VdW-induced downward and REGO-induced upward water migration. Increasing S_L (and hence permeability), either by increasing permafrost temperature or soil
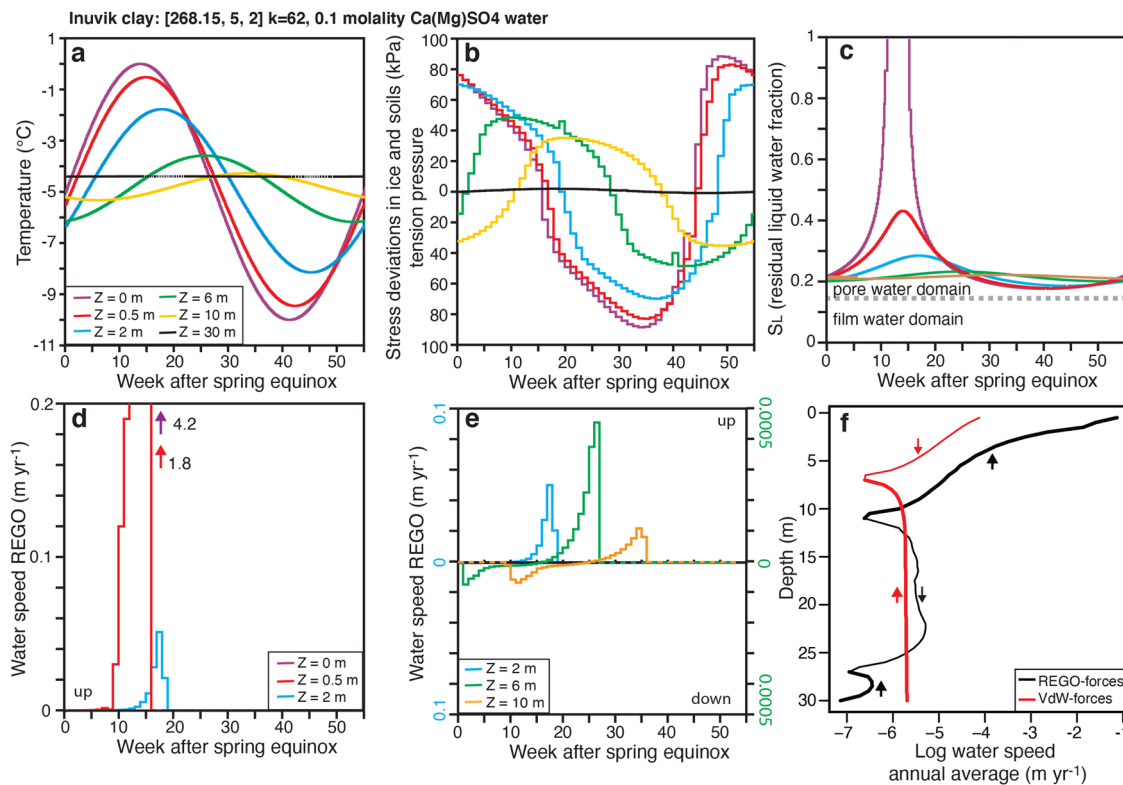
Fig. 4 Typical weekly variations in ground temperature, stress, and unfrozen water content, and the REGO-induced water speeds within Inuvik clay permafrost with Ca(Mg)SO$_4$ water chemistry. Weekly variations measured from the spring equinox in **a** ground temperature, **b** stress deviations in permafrost, **c** unfrozen water content, **d**, **e** maximum water speeds induced by REGO forces in 30 m Inuvik clay permafrost with Ca(Mg)SO$_4$ water chemistry, and **f** profiles of annual averages water speed from REGO forces and VdW forces up to 30 m depth. Data are presented from the spring equinox. Numerical simulation was performed for mean annual ground surface temperature of −5 °C, amplitude of 5 °C, and thermal diffusivity of 62 m^2 yr^{-1}. Table 3 lists values used in the WATEREGO simulation.

water salinity, would increase the rate at which ice can accumulate in the near-surface.

A first-order estimate of the time required to evolve the ground ice profiles at all three sites from the ensemble numerical simulations can be obtained from: $-1/(dWS_{REGO}/dZ)$, which has unit in years; the estimates are reasonable for the three sites. On the Peel Plateau/Richardson Mountains, permafrost aggraded in the clayey-silt tills following glacial retreat during the Late Pleistocene[18]. For the simulations using the 50:50 mixture of Navy Rd clayey silt and Inuvik clay and 265 K MAGST and Ca(Mg)SO$_4$ soil water, the evolved ground ice profile can be obtained in ~10,000 years, which is within the estimated age of permafrost in the Peel Plateau/Richardson Mountains region; increasing the temperature by 3° would reduce the time to reach the ground ice content profile to ~2000 years. At Friis Hills, the sediments were deposited 15–14 Ma[27,77] and the simulations using Fujinori soils and 250 K MAGST and 0.1× sea water soil solution, suggest that the ground ice content profile can be obtained within ~1 Myr. In lower Beacon Valley, no direct ages were obtained on the sediments; Cuozzo et al. estimated the age of the surface sediments to be > 1 Myr based on calculated sublimation rates in the central portion of Beacon Valley[48], a region where >8.1 Myr buried glacial ice was discovered[78]. For the simulations at lower Beacon Valley using Lebanon gravels and 250 K MAGST and 0.2× sea water soil solution, the ice-rich zone in the upper few meters below the ice table can be obtained within hundred thousands of years, but the ground ice profile below that depth can be obtained in ~25 Myr. This is much longer than the estimated age of the surface sediments. Increasing temperatures by 5° warmer (as evidenced from past warm climate intervals)

would increase the ice-build up rate by a factor of 2 in the uppermost 10 m. The simulation was performed using gravels, but the sediments contain ~5% clays, and this would increase S$_L$, permeability, and the rate at which the unfrozen water can migrate. Modeling suggests that these clays would become responsible for the bulk of the water motion through REGO forces and ice build-up rate would be 1/20th of full clay sediments or about 1 order of magnitude faster than in gravels only. This approaches the estimated age of the surface sediments, ~1 Myr.

Replacement age of intrasedimental ice in permafrost sediments. The near-surface permafrost sediments are commonly ice-rich with ice contents exceeding that of the deeper permafrost (Figs. 2 and 6). Two scenarios have been advanced to explain this development of ice-rich permafrost. The first is driven by external factors where climate cooling, addition of organic matter, or sedimentation causes the upward aggradation of permafrost and the development of ice lenses if the active layer is moist (i.e., ref. [71]). Conversely, at sites where active layer thicknesses have remained stable, it was proposed that VdW forces (internal factors) produce a net downward flux of soil water from the active layer into near-surface permafrost which results in the development of an ice-rich zone in the top of the permafrost. The latter has been shown to occur as well in silts to coarser material from our modeling. However, the rate at which ground ice can accumulate has remained largely unknown. Using WATEREGO, we explored how fast an initial ground ice content profile could evolve over time in the Inuvik clay, Chena silt, and Nagare peat
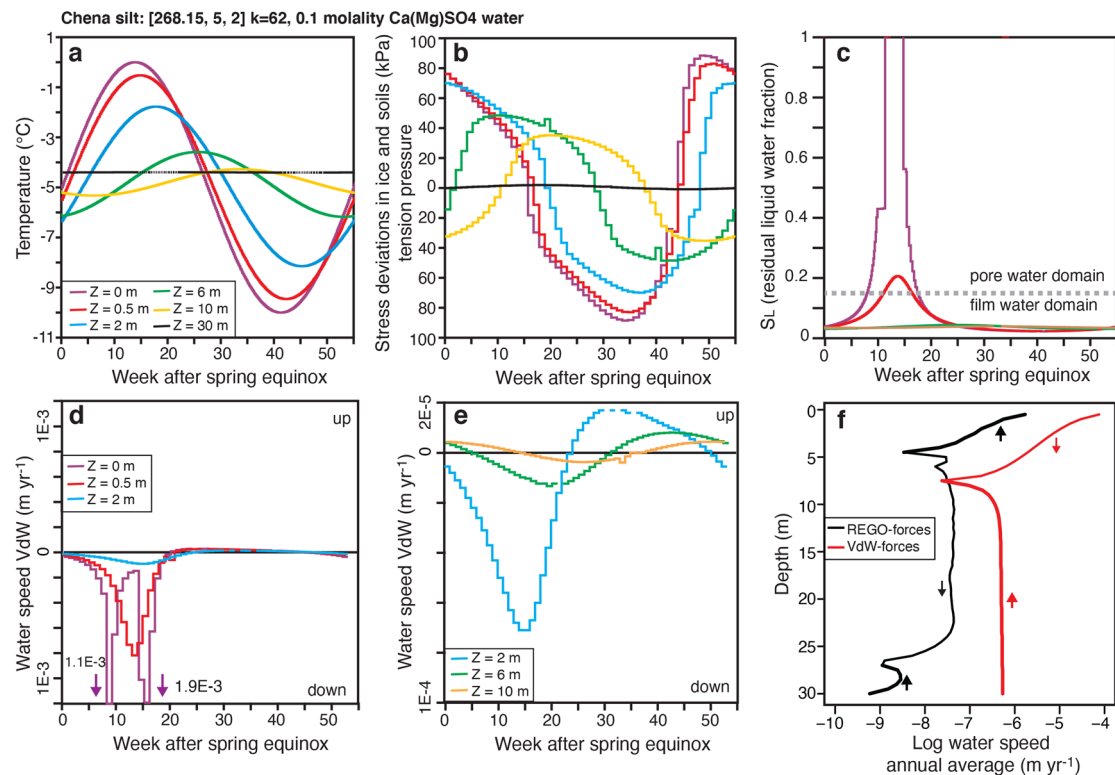
Fig. 5 Typical weekly variations in ground temperature, stress, and unfrozen water content, and the VdW-induced water speeds within Chena silt permafrost with Ca(Mg)SO$_4$ water chemistry. Weekly variation measured from the spring equinox in **a** ground temperature, **b** stress deviations in permafrost, **c** unfrozen water content, **d**, **e** maximum water speeds induced by VdW forces in 30 m Chena silt permafrost with Ca(Mg)SO$_4$ water chemistry, and **f** profiles of annual averages water speed from REGO forces and VdW forces up to 30 m depth. Numerical simulation was performed for mean annual ground surface temperature of –5 °C, amplitude of 5 °C, and thermal diffusivity of 62 m^2 yr^{-1}. Table 3 lists values used in the WATEREGO simulation.

with varying initial soil water chemistry (pure water to 1× sea-water). The values for the parameters used to generate the ensembles are listed in Table 3.

The replacement age is calculated as the inverse of the derivative of the net water speed with depth and adjusted by an e-folding function (1/2e to 1/7e) to account for the effect of changing ice content on porosity[28]. For clays, the replacement age of ice for 0.1 molality Ca(Mg)SO$_4$ chemistry in the uppermost 2.5 m ranges from 1 to 1000 years, but is in the order of 1000 years to 1 Myr for silts (Fig. 7). The Nagare peat has an intermediate replacement age (10–10,000 years) (Fig. 7). For the Inuvik clay, the dominant process in determining the replacement age of ice (for all soil chemistries) is the REGO forces. This is because S$_L$ is within the pore water domain (S$_L$ > ~0.13) and the permeability is therefore enhanced in relation to S$_L$ in the film water domain. For the Chena silt, the VdW forces (which move water at a much slower speed) are dominant for low salinity waters until 0.2× sea water salinity, at which point REGO and VdW processes are of similar importance. At higher salinity, the REGO forces become dominant due to increased S$_L$. Therefore, silts (and gravels) with water chemistry higher than 0.2× sea water can start to have a replacement age of ice in the range of clays with low salinity, and silts with salinity near that of sea water will have a replacement age equal to that of clays with the same salinity. This finding can explain why the permafrost sediments in the cold and hyper-arid stable upland zone of the MDV can have similar vertical ground ice profiles to sites in the warmer-wetter Arctic. Despite the colder temperatures, the sediments in the upper MDV have a salt content 1–4 orders of magnitude higher than along the coastal thaw zone of the MDV

or in the Arctic, which results in similar to higher S$_L$ in the permafrost sediments. Therefore, the results from our modeling suggest that ground ice content can increase over a relatively short period in clays (10–1000 years in the uppermost 1 m) with low salinity silts taking 1–2 orders of magnitude longer. If the salinity of silts and sands is higher (>0.5× seawater) the rate of accumulation would approach that of clays.

Re-defining frost susceptibility of sediments. The frost susceptibility of sediments is defined in terms of their frost-heaving and thaw-weakening behavior[14]. Traditionally, the frost susceptibility of a sediment has been based solely on particle size: with fine-grained sediments having a higher frost susceptibility (i.e., the Andersen-Tice S$_L$ functions)[79]. This is generally correct for Arctic permafrost sediments. However, sediments with increased salinity or that were exposed to sub-aerial conditions for > 100 kyr can become frost-susceptible. For example, the salt-rich sandy permafrost sediments in the upper MDV have been subjected to REGO and VdW forces for 100 s kyr to 15 Myr and the ground ice content in the uppermost 1 m at some sites is as high as in fine-grained sediments in the Arctic regions (Fig. 2). Therefore, given the right conditions (a combination of parameters that affect S$_L$, permeability, and water speeds), all sediment types could be classified as frost-susceptible, it's just that clays reach that state faster without the need of increased soil water salinity or ground temperatures. This has relevance for mapping the distribution of thaw sensitive permafrost and classification of abundance of intrasedimental ice should consider sediment type and soil water chemistry.
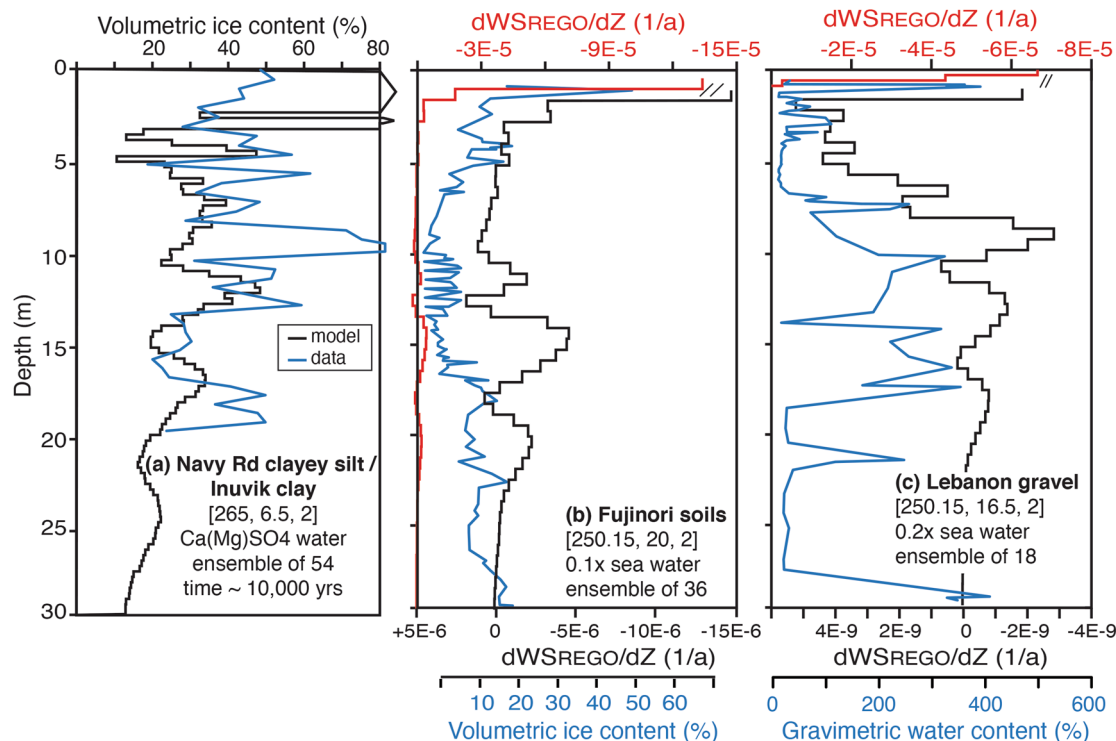
Fig. 6 Comparison of measured and modeled vertical distribution of ground ice in permafrost sediments. a Volumetric ice content profile in Richardson Mountains/Peel Plateau region in NWT[28] (shown is the median of ground ice volume from 10 permafrost cores and averaged in 0.5 m bin interval) compared with a 50:50 mixture of Chena silt and Inuvik clay type sediment. **b** Volumetric ice content profile at Friis Hills[27] compared with the negative depth derivatives of water speeds (dWS_{REGO}/dZ) of Fujinomori soil type. **c** Gravimetric ice content profile at Beacon Valley[26] compared with the negative depth derivatives of water speeds (dWS_{REGO}/dZ) of Lebanon gravel. The negative depth derivatives of water speeds (dWS_{REGO}/dZ) are used to indicate where ice accumulates by freezing or is removed by melting. Table 3 lists values of all parameters used in the WATEREGO ensemble simulation, in the square brackets are the mean annual ground surface temperature and its amplitude (in K) and the geothermal gradient (in K per 100 m). The colors of the lines in panels **b** and **c** correspond to the color of the x-axis titles. Note the change in scale for dWS_{REGO}/dZ in the upper few meters.

Table 3 Values of input parameters used in ensemble modeling with WATEREGO for Figs. 4–7.

Parameter	Component	Inuvik clay	Chena silt	Lebanon gravel	Nagare peat	Fujinomori soil
MAGST (K)	Thermal	265	265	250.15	268.15	250
T_{amp} (K)	Thermal	6.5	6.5	16.5	5.5	20
GRAD (K/100 m)	Thermal	2	2	2	2	2
DIFUST (m^2/yr)	Thermal	15, 30, 61.9	15, 30, 61.9	15, 30, 61.9	30	30, 62
Kpaterson	Creep	1	1	1	1	3
KTENSE	Tension	0	0	0	0	0
KTENS (VdW)	Tension	1	1	1	1	1
LINE #	Permeability	6	6	6	6	6
Hamaker constant (joules)	Permeability	−6.32 E−18	−6.32 E−18	−6.32 E−18	−6.32 E−17	−6.32 E−18
R_{soil} (µm)	Permeability	1	5	100	10	1, 10, 100
S_{Lthrsh}	Permeability	0.21, 0.17, 0.13	0.17, 0.13	0.13	0.075, 0.13, 0.06	0.17, 0.13
FDIN	Porosity	0.20, 0.42, 0.55	0.20, 0.42, 0.55	0.42, 0.55	0.9, 0.76	0.42, 0.5
KBASE	Water chemistry	Ca(Mg)SO$_4$	Ca(Mg)SO$_4$	seawater	Ca(Mg)SO$_4$	seawater
FRACTB	Chemistry strength	1	1	0.2	1	0.1

Conclusion

The current ground ice and permafrost geohazard maps rely on the frost susceptibility of surficial sediments. Large areas of these maps under-estimate ground ice abundance. Here we demonstrate the importance of considering the Rempel-type S_L (a parameter dependent on sediment type, soil water chemistry, and temperature) when assessing the frost susceptibility of permafrost sediments. With knowledge of sediment type, soil water chemistry, MAGST, and its amplitude, the WATEREGO soil environmental model is able to match reasonably well the vertical distribution of ground ice in Arctic or Antarctic permafrost sediments. As such, the ensemble model could be used to produce a comprehensive estimate of the vertical distribution of intrasedimental ice in permafrost sediments at regional scale and improving geohazard risk assessments. The modeling of the vertical migration of water through sediments can also be used to assess the mobilization and concentration of salts both of which have implication for habitability and microbial activity in permafrost.
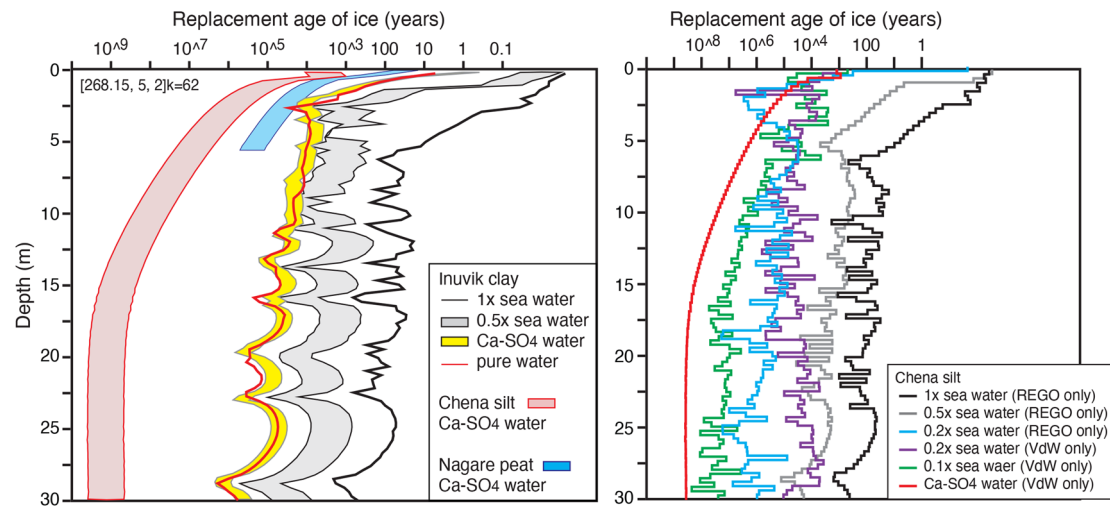
Fig. 7 Replacement age of ground ice in various sediments and soil water chemistries. Table 3 lists values used in the WATEREGO ensemble simulations. The replacement age is calculated as the inverse of the derivative of the net water speed with depth and adjusted by an e-folding function (1/2e to 1/7e) to account for the effect of changing ice content on porosity.

Methods

Numerical modeling. Here, we provide the relevant equations to determine the unfrozen water content, the water speeds in permafrost sediments and replace age of ice using WATEREGO. The complete details of the ensemble numerical modeling are presented in ref. [28].

Unfrozen water content. The unfrozen water content profiles (S_L) in relation with soil temperature, soil porosity, dry bulk density, and soil water chemistry were determined from:

$$S_L = \left(\frac{T_L + Tp - T}{\Delta T_f}\right)^{-\beta} \text{ (if SL > 1.0 then it is set to1.0)} \quad (1)$$

where S_L is the fraction of residual unfrozen water with respect to total volume of water (water and ice), T_L is the freezing temperature of the soil water (in K), Tp (in K) is a correction to T_L due to dry porosity, T is the temperature of the icy soil (in K), ΔT_f is the temperature difference across the freezing fringe in the soil-water system and β is a soil specific empirical constant.

The values for β and ΔT_f can be calculated from:

$$\beta = -B, \text{ and} \quad (2)$$

$$\Delta T_f = A^B \left(\frac{\rho_{ice} \times f}{\rho_{drysoil}}\right)^{-B} \quad (3)$$

where A and B are fit parameters from Andersland and Ladanyi[79], f is soil porosity, ρ_{ice} is density of the ice (in kg m^{-3}) and $\rho_{drysoil}$ is dry soil density (in kg m^{-3}). The fit parameters can be calculated for any soils by conducting an Atterberg liquid-limit test[14,80]. Values of parameters used in this study are listed in Table 1.

Water speeds. The speed at which pore water in a coupled soil thermal and pressure gradient (REGO forces) will move can be determined by:

$$w = -\left(\frac{perm}{\mu}\right)\frac{dp}{dz} \quad (4)$$

where w is the bulk fluid speed (m yr^{-1}) (ref. [81]), "perm" is the permeability of the fluid (m^2), μ is the dynamic viscosity of the fluid (N m^{-2} yr^{+1}) and near 0 °C it is 5.6866 10^{-11} N (m^{-2} yr^{-1}; ref. [82]), p is pressure (Pa), and z is the depth measured (+ downwards).

The permeability of water film (VdW forces) can then be determined from:

$$perm_{fw} = \frac{-A}{36 * \pi * R}\left[\rho L \frac{T_L - T}{T_L} + \frac{2\gamma_{sl}}{R}\right]^{-1}(1 - f_d) \quad (5)$$

where A is the Hamaker constant whose value is specific to the soil type (in J) (ref.[83]), R is the radius of the soil particle (in m), ρ is the density of water (in kg m^{-3}), L the latent heat of fusion (in J kg^{-1}), T_L is the melting temperature of the water (without soil, in K), T is the ambient temperature (in K), γ_{sl} is the surface energy of the solid-liquid interface (specific to soil type, in J m^{-2}) and f_d is the dry porosity.

Replacement age of intrasedimental ice. The replacement age is calculated as the inverse of the derivative of the net water speed with depth and adjusted by

an e-folding function (1/2e to 1/7e) to account for the effect of changing ice content on porosity[28]. The replacement age (units of time in years) is calculated as:

$$\left|f_D\left(-\frac{dW_s}{dZ}\right)^{-1}\right| \quad (6)$$

Since the time can lead to either pure ice or no ice, we use the absolute value.

The changing rate of ice build-up or removal is adjusted by this e-folding function:

$$ave\left\{\frac{dWs}{dZ}\right\} = \frac{\tau}{t_m}\left(\frac{dWs}{dZ}\right)_o\left(1 - e^{\frac{-t_m}{\tau}}\right) \quad (7)$$

Data availability

Code availability

References

1. Biskaborn, B. K. et al. Permafrost is warming at a global scale. *Nat. Commun.* **10**, 264 (2019).
2. Jin, X.-Y. et al. Impacts of climate-induced permafrost degradation on vegetation: a review. *Adv. Clim. Chang. Res.* **12**, 29–47 (2021).
3. Lafrenière, M. J. & Lamoureux, S. F. Effects of changing permafrost conditions on hydrological processes and fluvial fluxes. *Earth-Sci. Rev.* **191**, 212–223 (2019).
4. Herndon, E., Kinsman-Costello, L. & Godsey, S., Biogeochemical cycling of redox-sensitive elements in permafrost-affected ecosystems. In *Biogeochemical Cycles: Ecological Drivers and Environmental Impact* 245–265 (Wiley, 2020). https://doi.org/10.1002/9781119413332.ch12
5. Schaefer, K., Lantuit, H., Romanovsky, V. E., Schuur, E. A. G. & Witt, R. The impact of the permafrost carbon feedback on global climate. *Environ. Res. Lett.* **9**, 085003 (2014).
6. Schuur, E. A. G. et al. Climate change and the permafrost carbon feedback. *Nature* **520**, 171–179 (2015).

7. Guan, X. J., Spence, C. & Westbrook, C. J. Shallow soil moisture–ground thaw interactions and controls–Part 2: influences of water and energy fluxes. *Hydrol. Earth Syst. Sci.* **14**, 1387–1400 (2010).

8. Jorgenson, M. T. et al. Resilience and vulnerability of permafrost to climate change. *Can. J. For. Res.* **40**, 1219–1236 (2010).

9. Smith, S. L., Burgess, M. M. & Heginbottom, J. A. Permafrost in Canada, a challenge to northern development. In *A synthesis of geological hazards in Canada* (ed. Brooks, G. R.) 241–264 (Geological Survey of Canada, Bulletin 548, 2001).

10. Karjalainen, O. et al. Circumpolar permafrost maps and geohazard indices for near-future infrastructure risk assessments. *Sci. Data* **6**, 190037 (2019).

11. Pollard, W., Periglacial processes in glacial environments. In *Past Glacial Environments* 537–564 (Elsevier, 2018). https://doi.org/10.1016/B978-0-08-100524-8.00016-6

12. Mackay, J. R. The world of underground ice. *Ann. Assoc. Am. Geogr.* **62**, 1–22 (1972).

13. Jorgenson, M. T. & Grosse, G. Remote sensing of landscape change in permafrost regions. *Permafr. Periglac. Process* **27**, 324–338 (2016).

14. Aderslund, O. & Ladanyi, B. *Frozen Ground Engineering.* (John Wiley & Sons, 2004).

15. Heginbottom, J., Dubreuil, M. & Haker, P. Canada permafrost, 1:7,500,000 scale. *National Atlas Canada, 5th Ed. Sheet MCR 4177* (1995).

16. O'Neill, H. B., Wolfe, S. A. & Duchesne, C. New ground ice maps for Canada using a paleogeographic modelling approach. *Cryosphere* **13**, 753–773 (2019).

17. Bockheim, J. G., Campbell, I. B. & McLeod, M. Permafrost distribution and active-layer depths in the McMurdo Dry Valleys. *Antarctica. Permafr. Periglac. Process.* **18**, 217–227 (2007).

18. Lacelle, D., Bjornson, J., Lauriol, B., Clark, I. D. & Troutet, Y. Segregated-intrusive ice of subglacial meltwater origin in retrogressive thaw flow headwalls, Richardson Mountains, NWT, Canada. *Quat. Sci. Rev.* **23**, 681–696 (2004).

19. Lacelle, D., Fontaine, M., Pellerin, A., Kokelj, S. V. & Clark, I. D. Legacy of holocene landscape changes on soil biogeochemistry: a perspective from paleo-active layers in Northwestern Canada. *J. Geophys. Res. Biogeosciences* **124**, 2662–2679 (2019).

20. Kotler, E. & Burn, C. R. Cryostratigraphy of the Klondike" muck" deposits, west-central Yukon Territory. *Can. J. Earth Sci.* **37**, 849–861 (2000).

21. French, H. M. H. & Pollard, W. H. Ground-ice investigations, Klondike District, Yukon Territory. *Can. J. Earth* **23**, 550–560 (1986).

22. De Pascale, G. P., Pollard, W. H. & Williams, K. K. Geophysical mapping of ground ice using a combination of capacitive coupled resistivity and ground-penetrating radar, Northwest Territories, Canada. *J. Geophys. Res. Earth Surf.* **113**, 1–15 (2008).

23. Angelopoulos, M. C., Pollard, W. H. & Couture, N. J. The application of CCR and GPR to characterize ground ice conditions at Parsons Lake, Northwest Territories. *Cold Reg. Sci. Technol.* **85**, 22–33 (2013).

24. Fortier, R., Allard, M., Gagnon, O. & LeBlanc, A.-M. Assessment of permafrost conditions at Salluit, Nunavik, using cone penetration tests. in *Proceedings of the 57th Canadian Geotechnical Conference* 39–48 (Canadian Geotechnical Society, 2004).

25. Lapalme, C. et al. Distribution and origin of ground ice in University Valley, McMurdo Dry Valleys, Antarctica. *Antarct. Sci.* **29**, 183–198 (2017).

26. Cuozzo, N. et al. Silicate weathering in antarctic ice-rich permafrost: insights using magnesium isotopes. *Geochim. Cosmochim. Acta* **278**, 244–260 (2020).

27. Verret, M. et al. Cryostratigraphy of mid-Miocene permafrost at Friis Hills, McMurdo Dry Valleys of Antarctica. *Antarct. Sci.* **33**, 174–188 (2021).

28. Fisher, D. A., Lacelle, D. & Pollard, W. A model of unfrozen water content and its transport in icy permafrost soils: effects on ground ice content and permafrost stability. *Permafr. Periglac. Processes* **31**, 184–199 (2020).

29. Horiguchi, K. & Miller, R. D. Hydraulic conductivity of frozen earth materials. In *4th International Conference on Permafrost* 504–509 (National Academic Press, 1983).

30. Hansson, K., Šimůnek, J., Mizoguchi, M., Lundin, L.-C. & van Genuchten, M. T. Water flow and heat transport in frozen soil: Numerical solution and freeze-thaw applications. *Vadose Zone J.* **3**, 693–704 (2004).

31. Watanabe, K. & Flury, M. Capillary bundle model of hydraulic conductivity for frozen soil. *Water Resour. Res.* **44**, W12402 (2008).

32. Bing, H., He, P. & Zhang, Y. Cyclic freeze-thaw as a mechanism for water and salt migration in soil. *Environ. Earth Sci.* **74**, 675–681 (2015).

33. Müeller, S. W. *Permafrost or permanently frozen ground and related engineering problems.* (US Geological Survey Special Report Special no. 62, 1945).

34. Brown, R. J. E. & Kupsch, W. O. *Permafrost terminology. Technical Memorandum (National Research Council of Canada. Associate Committee on Geotechnical Research); no. 111* (National Research Council of Canada. Associate Committee on Geotechnical Research, 1974). https://doi.org/10.4224/20378592

35. Anderson, D. M. & Morgenstern, N. R. Physics, chemistry and mechanics of frozen ground: a review. In *Proceeding Second Internal conference on permafrost* 257–288 (National Academy of Science, 1973).

36. van Everdingen, R. O. Geocryological terminology. *Can. J. Earth Sci.* **13**, 862–867 (1976).

37. Pewe, T. L. Sand-wedge polygons (tesselations) in the McMurdo Sound region, Antarctica; a progress report. *Am. J. Sci.* **257**, 545–552 (1959).

38. Campbell, I. B., Claridge, G. G., Balks, M. R. & Campbell, D. Permafrost properties in the McMurdo Sound-Dry Valley region of Antarctica. in *Permafrost-Seventh International Conference (Proceedings)* (eds. Lewkowicz, A. G. & Allard, M.) 121–126 (Collection Nordicana No. 55, 1998).

39. Bockheim, J. G. & Tarnocai, C. Nature, occurrence and origin of dry permafrost. in *Permafrost–Seventh International Conference (Proceedings)* (eds. Lewkowicz, A. G. & Allard, M.) 57–64 (Collection Nordicana No. 55, 1998).

40. Adlam, L. S., Balks, M. R., Seybold, C. A. & Campbell, D. I. Temporal and spatial variation in active layer depth in the McMurdo Sound Region, Antarctica. *Antarct. Sci.* **22**, 45 (2010).

41. Guglielmin, M. Ground surface temperature (GST), active layer and permafrost monitoring in continental Antarctica. *Permafr. Periglac. Process.* **17**, 133–143 (2006).

42. Mellon, M. T. et al. Ground ice at the Phoenix Landing Site: Stability state and origin. *J. Geophys. Res.* **114**, E00E07 (2009).

43. Lapalme, C. M. et al. Cryostratigraphy and the sublimation unconformity in permafrost from an ultraxerous environment, University Valley, McMurdo Dry valleys of Antarctica. *Permafr. Periglac. Process* **28**, 649–662 (2017).

44. Kurylyk, B. L. & Hayashi, M. Improved Stefan equation correction factors to accommodate sensible heat storage during soil freezing or thawing. *Permafr. Periglac. Process* **27**, 189–203 (2016).

45. Fisher, D. A., Lacelle, D., Pollard, W., Davila, A. F. & McKay, C. P. Ground surface temperature and humidity, ground temperature cycles and the ice table depths in University Valley, McMurdo Dry Valleys of Antarctica. *J. Geophys. Res. Earth Surf.* **121**, 2069–2084 (2016).

46. McKay, C. P., Mellon, M. T. & Friedmann, E. I. Soil temperatures and stability of ice-cemented ground in the McMurdo Dry Valleys, Antarctica. *Antarct. Sci.* **10**, 31–38 (1998).

47. Hagedorn, B., Sletten, R. S. & Hallet, B. Sublimation and ice condensation in hyperarid soils: modeling results using field data from Victoria Valley, Antarctica. *J. Geophys. Res.* **112**, F03017 (2007).

48. Liu, L. et al. An enhanced model of the contemporary and long-term (200 ka) sublimation of the massive subsurface ice in Beacon Valley, Antarctica. *J. Geophys. Res. Earth Surf.* **120**, 1596–1610 (2015).

49. Shi, Y., Niu, F., Lin, Z. & Luo, J. Freezing/thawing index variations over the circum-Arctic from 1901 to 2015 and the permafrost extent. *Sci. Total Environ.* **660**, 1294–1305 (2019).

50. Smith, S. L. et al. Thermal state of permafrost in North America: a contribution to the international polar year. *Permafr. Periglac. Process* **21**, 117–135 (2010).

51. Kokelj, S. V. & Burn, C. R. Geochemistry of the active layer and near-surface permafrost, Mackenzie delta region, Northwest Territories, Canada. *Can. J. Earth Sci.* **42**, 37–48 (2005).

52. Pollard, W. H. Distribution and characterization of ground ice on Fosheim Peninsula, Ellesmere Island, Nunavut. *Bull. Geol. Surv. Can.* (2000). https://doi.org/10.4095/211959

53. Pollard, W., Ward, M. & Becker, M. The Eureka Sound lowlands: an ice-rich permafrost landscape in transition. In *68e Conférence Canadienne de Géotechnique et 7e Conférence Canadienne sur le Pergélisol, 20 au 23 septembre 2015, Québec, Québec.* (2015).

54. Tarasov, L., Dyke, A. S., Neal, R. M. & Peltier, W. R. A data-calibrated distribution of deglacial chronologies for the North American ice complex from glaciological modeling. *Earth Planet. Sci. Lett.* **315–316**, 30–40 (2012).

55. Dyke, A. S. Late quaternary vegetation history of northern North America based on pollen, macrofossil and faunal remains. *Geogr. Phys. Quat.* **59**, 211–262 (2005).

56. Smith, I. R. & Lesk-Winfield, K. *An updated assessment of ground ice and permafrost geology-related observations based on seismic shothole drillers' log records, Northwest Territories and northern Yukon.* (2012). https://doi.org/10.4095/290974

57. Hodgson, D. A. & Nixon, F. M. *Ground ice volumes determined from shallow cores from western Fosheim peninsula Ellesmere island, northwest territories. Bulletin of the Geological Survey of Canada* (Government of Canada, 1998).

58. Levy, J. How big are the McMurdo Dry Valleys? Estimating ice-free area using Landsat image data. *Antarct. Sci.* **25**, 119–120 (2013).

59. Obryk, M. K., Doran, P. T., Fountain, A. G., Myers, M. & McKay, C. P. Climate from the McMurdo Dry Valleys, Antarctica, 1986–2017: surface air temperature trends and redefined summer season. *J. Geophys. Res. Atmos.* **125**, e2019JD032180 (2020).

60. Fountain, A. G., Nylen, T. H., Monaghan, A., Basagic, H. J. & Bromwich, D. Snow in the McMurdo Dry Valleys. *Antarctica. Int. J. Climatol.* **30**, 633–642 (2010).

61. Denton, G. H., Sugden, D. E., Marchant, D. R., Hall, B. L. & Wilch, T. I. East Antarctic ice sheet sensitivity to pliocene climatic change from a dry valleys perspective. *Geogr. Ann. Ser. A Phys. Geogr.* **75**, 155 (1993).

62. Lacelle, D. et al. Solar radiation and air and ground temperature relations in the cold and hyper-arid Quartermain Mountains, McMurdo Dry Valleys of Antarctica. *Permafr. Periglac. Process.* **27**, 163–176 (2016).

63. Vieira, G. et al. Thermal state of permafrost and active-layer monitoring in the antarctic: advances during the international polar year 2007-2009. *Permafr. Periglac. Process.* **21**, 182–197 (2010).

64. Marchant, D. R., Denton, G. H., Bockheim, J. G., Wilson, S. C. & Kerr, A. R. Quaternary changes in level of the upper Taylor Glacier, Antarctica: implications for paleoclimate and East Antarctic Ice Sheet dynamics. *Boreas* **23**, 29–43 (2008).

65. Claridge, G. G. & Campbell, I. B. The salts in Antarctic soils, their distribution and relationship to soil processes. *Soil Sci.* **123**, 377–384 (1977).

66. Balks, M. R., Campbell, D., Campbell, I. B. & Claridge, G. G. *Interim results of 1993/94 soil climate, active layer and permafrost investigations at Scott Base, Vanda and Beacon Heights, Antarctica.* (1995).

67. Campbell, I. B., Claridge, G. G. C. & Balks, M. R. Short- and long-term impacts of human disturbances on snow-free surfaces in Antarctica. *Polar Rec.* **34**, 15–24 (1998).

68. Campbell, I. B. Soil characteristics at a long-term ecological research site in Taylor Valley. *Antarct. Soil Res.* **41**, 351–364 (2003).

69. Gilichinsky, D. A. et al. Microbial populations in Antarctic permafrost: biodiversity, state, age, and implication for astrobiology. *Astrobiology* **7**, 275–311 (2007).

70. Dickinson, W. W., Schiller, M., Ditchburn, B. G., Graham, I. J. & Zondervan, A. Meteoric Be-10 from Sirius Group suggests high elevation McMurdo Dry Valleys permanently frozen since 6Ma. *Earth Planet. Sci. Lett.* **355–356**, 13–19 (2012).

71. Cheng, K. The mechanism of repeated-segregation for the formation of thick layered ground ice. *Cold Reg. Sci. Technol.* **8**, 57–66 (1983).

72. Anderson, D. M. & Tice, A. R. Predicting unfrozen water contents in frozen soils from surface area measurements. *Highw. Res. Rec.* **373**, 12–18 (1972).

73. Rempel, A. W. A theory for ice-till interactions and sediment entrainment beneath glaciers. *J. Geophys. Res.* **113**, F01013 (2008).

74. Sizemore, H. G. & Mellon, M. T. Laboratory characterization of the structural properties controlling dynamical gas transport in Mars-analog soils. *Icarus* **197**, 606–620 (2008).

75. Burn, C. R. & Michel, F. A. Evidence for recent temperature-induced water migration into permafrost from the tritium content of ground ice near Mayo, Yukon Territory, Canada. *Can. J. Earth Sci.* **25**, 909–915 (1988).

76. Chizhov, A., Chizhova, N., Morkovina, I. & Romanov, V. Tritium in permafrost and ground ice. In *4th International Conference on Permafrost* 1030–1035 (National Academy Press, 1983).

77. Lewis, A. R. & Ashworth, A. C. An early to middle Miocene record of ice-sheet and landscape evolution from the Friis Hills, Antarctica. *Geol. Soc. Am. Bull.* **128**, 719–738 (2016).

78. Marchant, D. R. et al. Formation of patterned ground and sublimation till over Miocene glacier ice in Beacon Valley, southern Victoria Land, Antarctica. *Geol. Soc. Am. Bull* **114**, 718–730 (2002).

79. Andersland, O. B. & Ladanyi, B. Frozen Ground Chapter 1. In *Frozen Ground Engineering, 2nd Edition* (2004).

80. Banin, A. & Anderson, D. M. Effects of salt concentration changes during freezing on the unfrozen water content of porous materials. *Water Resour. Res.* **10**, 124–128 (1974).

81. Hindmarsh, R. C. A., van der Wateren, F. M. & Verbers, A. L. L. Sublimation of ice through sediment in Beacon Valley, Antarctica. *Geogr. Ann. Ser. A Phys. Geogr.* **80**, 209–219 (1998).

82. Poling, B., Prausnitz, E. & O'Connell, J. *The Properties of Gases and Liquids.* (McGraw-Hill, 2001).

83. Rempel, A. W., Wettlaufer, J. S. & Worster, M. G. Premelting dynamics in a continuum model of frost heave. *J. Fluid Mech.* **498**, 227–244 (2004).

84. Nagare, R. M., Schincariol, R. A., Quinton, W. L. & Hayashi, M. Effects of freezing on soil temperature, freezing front propagation and moisture redistribution in peat: Laboratory investigations. *Hydrol. Earth Syst. Sci.* **16**, 501–515 (2012).

85. Environment Canada. Canadian Climate Normals 1981-2010 Station Data. (2010). Available at: http://climate.weather.gc.ca. (Accessed: 23rd February 2016)

86. Marchant, D. R. & Head, J. W. Antarctic dry valleys: microclimate zonation, variable geomorphic processes, and implications for assessing climate change on Mars. *Icarus* **192**, 187–222 (2007).

Acknowledgements

Author contributions

D.L., D.A.F., W.P. conceived the study; D.L., M.V. acquired data; D.A.F. developed the numerical modeling; all contributed to drafting and revising the manuscript.

Competing interests

The authors declare no competing interests.

Additional information

Supplementary information The online version contains supplementary material available at https://doi.org/10.1038/s43247-022-00367-z.

Correspondence and requests for materials should be addressed to Denis Lacelle.

Peer review information *Communications Earth & Environment* thanks Melisa Diaz and the other, anonymous, reviewer(s) for their contribution to the peer review of this work. Primary Handling Editors: Jan Lenaerts and Clare Davis.

Reprints and permission information is available at http://www.nature.com/reprints

Publisher's note Springer Nature remains neutral with regard to jurisdictional claims in published maps and institutional affiliations.